Génie biomédical
Biomedical Engineering

DETECTION OF PARKINSON'S DISEASE VIA CLIFFORD GRADIENT-BASED RECURRENT NEURAL NETWORK USING MULTI-DIMENSIONAL DATA

ARUN RAMAIAH[1], PARVATHI DEVI BALASUBRAMANIAN[2], AHILAN APPATHURAI[3],
NARAYAN APERUMAL MUTHUKUMARAN[4]

Disease prediction is a vital step in the early diagnosis of many diseases in the overpopulated modern world. The prediction has gotten simpler due to advancements in various machine learning (ML) techniques. However, the complexity of the model and the choice of the best machine-learning method for the given dataset significantly impact its accuracy. Globally, there are many datasets, but their unstructured nature prevents them from being used in any useful way. To extract anything valuable for use in the actual world, various strategies are therefore accessible. To evaluate the model, accuracy now serves as a key metric. This research proposes a novel Cliff-PD to detect Parkinson's disease using a Clifford gradient RNN classifier with MRI and EEG signals. Initially, the MRI images are denoised using multi-scale Retinex (MSR), and the EEG signal is denoised using Stationary Wavelet Transform filters to reduce the noise artifacts. Then, the Clifford Gradient RNN is employed to classify the normal, Non-specific white matter hyperintensity and global brain atrophy using MRI images. Furthermore, the Clifford Gradient RNN is employed to classify the normal, generalized background slowing using an EEG signal. The performance of the proposed Cliff-PD model achieved an accuracy of 99.18 %. Compared with SVMs, AlexNet's, and CROWD autoencoder, the accuracy range is improved overall by 5.38 %, 10.36 %, and 3.2 %, respectively.

1. INTRODUCTION

The second most prevalent neurological ailment is Parkinson's disease (PD), which affects more than 6 million individuals globally. PD is one of the primary causes of neurological impairment, and during the past 30 years, its prevalence has increased by a factor of 2.5 [1]. Brain cell loss in the substantia nigra and other areas is linked to Lewy bodies and Lewy neurites, which are characteristic of Parkinson's disease. PD is categorized as a synucleinopathy because Lewy bodies are mostly made up of aggregated and misfolded -synuclein species [2]. According to Braak and colleagues, the Lewy pathology pattern is believed to begin in the caudal brainstem and move rostrally to the upper brainstem, limbic areas, and eventually the neocortex. Though certainly not widespread, such spread exists. Potential disease-progression pathways include permissive synuclein templating, cell-to-cell transmission, and prions-like traits [3].

Over the past five years, clinical diagnostic criteria intended to improve Parkinson's disease diagnosis accuracy have been validated. A clear diagnosis cannot be made from the early stages due to tests or biomarkers, and clinical symptoms of this disorder can overlap with those of other neurodegenerative diseases [4]. As a result, even when the illness has fully developed, clinical diagnostic accuracy is still below ideal. Prodromal sickness diagnosis is required since this is when future disease-modifying drugs will have the highest potential of being effective [5]. Finally, it is necessary to characterize the many subtypes of PD more clearly, each of which requires a unique strategy for therapy due to its unique clinical presentation, prognosis, and underlying disease processes. Monogenic Parkinson's disease is the most prominent example, and there are now clinical trials testing subtype-specific treatments for this condition [6].

Analysis of medical imaging, particularly dopamine transporter scans (DaTscans) and magnetic resonance images (MRIs) [7], can be used to predict the development of PD. The primary goal of MRI analysis is to identify morphological differences in different brain regions, with particular attention paid to the volume of the lenticular nucleus, head of the caudate nucleus, and surface of the substantia nigra [8]. Single photon emission computer tomography is used to create DaT scans, and patients are given 123-I-Ioflupane before the scans are taken. Whether dopaminergic neurons in the substantia nigra are degenerating may be determined using DaTscans [9]. The regions around the caudate nucleus head are chosen and compared to the cerebellum, and ratios of specified volumes are calculated and used to diagnose Parkinson's disease. These areas are centered on the images and scans that are thought to be the most typical and used to create predictions [10]. When creating models for PD prediction, several data sources, such as imaging, genetics, clinical, and demographic data, are considered. Measurements of handwriting were used in other methods to diagnose Parkinson's. A potential method for diagnosing the condition has been developed based on handwriting measures taken from PD patients. It has been demonstrated that including age and sex information in the decision-making process improves PD diagnosis [11]. The key contribution of the research is summarized as,

- This research proposes a novel Cliff-PD to detect Parkinson's disease using a Clifford gradient recurrent neural networks (RNN) classifier with model images like MRI and EEG signals.
- The MRI images are initially denoised using MSR, and EEG signals are pre-processed using stationary wavelet transform filters to reduce noise artifacts.

[1] P.S.R Engineering College, Sivakasi, India. E-mail: arun.r@psr.edu.in
[2] Sri Sarada College for Women (Autonomous)Tirunelveli, India. E-mail: parvathi54@gmail.com
[3] PSN College of Engineering and Technology, Tirunelveli, India. E-mail: akhilanappathurai@psncet.ac.in
[4] Sri Eshwar College of Engineering, Coimbatore, India. E-mail: muthukumaran.n@sece.ac.in

- Then, the Clifford gradient RNN is employed to classify normal, non-specific white matter hyperintensity and global brain atrophy using MRI images.
- Furthermore, the Clifford gradient RNN is employed to classify the normal, generalized background slowing using an EEG signal.

The remaining components of this work were divided into the next five categories. The literature review is presented in section 2, the suggested strategy is discussed in section 3, the findings and analysis are shown in section 4, and the conclusion and recommendations for more studies are presented in section 5.

2. LITERATURE SURVEY

One of the most prevalent and fatal brain conditions, Parkinson's disease, has a devastating effect on many people's lives and has claimed many of them. Diverse literature works have been written about recent developments in deep learning and machine learning techniques.

In [12] a PD diagnosis based on ML was provided. The steps for feature selection and classification make up the suggested diagnostic approach. The feature selection challenge was approached using the Recursive Feature Elimination and Feature Importance techniques. The tests to categorize Parkinson's patients utilized Support Vector Machines, Regression Trees, and Artificial Neural Networks. It was shown that recursive feature removal in SVMs outperformed the other methods. The accuracy percentage for Parkinson's diagnosis with the fewest vocal characteristics was 93.84 %.

In [13] two convolutional neural network-based classification frameworks for PD based on sets of vocal (voice) features were suggested. Leave-one-person-out cross-validation (LOPO CV) assesses the proposed models. The method was trained on data from the UCI ML repository. The F-measure and Matthews's correlation data include an unbalanced distribution of classes. Thus, coefficient metrics are employed for assessment in addition to accuracy. Extracted deep features effectively improve the discriminative ability of the classifiers and successfully separate PD patients from healthy individuals.

In [14] was suggested a deep learning neural network to attempt to categorize the MR pictures of healthy controls and PD cases. For a more accurate diagnosis of PD, AlexNet's CNN architecture is employed. The MR images are used to train and assess the transfer learning network's accuracy metrics. With the suggested system, an accuracy of 88.9 % is attained. Shortly, DL algorithms will produce an objective and superior patient group classification that will aid doctors in diagnosing PD.

In [15] it was suggested to introduce an ideal feature selection technique based on DL and ACSA. The CROWD autoencoder model is evaluated using three feature selection techniques for six supervised classification strategies. The findings show that the CROWD autoencoder feature selection model better diagnoses PD than the mRMR, RFE, and CFS feature selection approaches. The healthcare industry will benefit from this research since it will improve categorization accuracy by 0.96 %.

In [16] was developed a method for diagnosing PD using a ResNet architecture originally designed for image classification and vowels with prolonged phonation. 100 patients (50 healthy and 50 with PD) comprise the PD dataset (from the PC-GITA database). Three instances were noted for each patient. Compared to the most recent state-of-the-art methods, the obtained accuracy on the validation set is over 90 %. The findings are encouraging because they showed that features picked up from studying natural images may be applied to synthetic images representing the speech signal's spectrogram.

In [17], six machine learning models each employ BO to optimize their hyperparameters were proposed. The target feature's class label is 1 and 0, with 1 denoting someone with Parkinson's disease and 0 denoting someone without the condition. Six machine learning models were tested for efficacy on the dataset before and after the hyperparameter tuning method. The experimental findings showed that the SVM model outperformed rival ML models before and after the hyperparameter tweaking approach. It uses BO to get an accuracy rate of 92.3 %.

In [18] was developed an effective, dependable method for automatically differentiating between individuals with PD and healthy controls (HC). To improve generalization capacity, three strategies are employed: early halting, data augmentation, and the synthetic minority over-sampling method (SMOTE). Focusing the PD-ResNet train on the difficult instances and removing the anomalous data creates a more precisely targeted loss function to improve classification performance further. Additionally, in classifying PD at various severity levels, the F1-score, accuracy, precision, recall, specificity, and recall are 92.03 %, 94.29 %, 90.41 %, 93.85 %, and 92.31 %, respectively.

In [19] a random forest (RF) classifier on PD, and a disease prediction strategy were suggested. A high-dimensional dataset with 754 attributes was used to evaluate Random Forest classification. A feature reduction strategy is utilized with the ANN model, increasing accuracy. The feature reduction strategy used with the classifier model that guarantees high accuracy will determine this. Our comparison of this model's accuracy to that of an ANN model that used PCA revealed a clear distinction. The model achieved a notable accuracy of up to 90 %.

In [20] it was presented a new framework for assessing PD gait patterns with cutting-edge deep-learning techniques. Three methods utilized in the study are (i) the energy content of the gait signals in the frequency domain is captured using spectrograms, (ii) GRU networks to incorporate temporal information, and (iii) a new architecture based on CNNs and GRUs to simultaneously capture spectral and temporal information [24–27]. The classification of PD vs. EHC and PD vs YHC was found to have accuracy levels of up to 83.7 % and 92.7 %, respectively.

In [21] was developed a machine-learning method for telemedicine to recognize PD at an early stage. The research was conducted using 30 PWP and healthy individuals' MDVP audio data while four ML models were being trained. random forest classifier using ML approach for the identification of PD, according to a comparison of classification results using SVM, RF, KNN, and logistic regression models. RF classifier model has a sensitivity of 0.95 and a detection accuracy of 91.83 %. The use of ML in telemedicine, through the findings of this paper, gives PD patients a new lease of life [22,23].

From the literature, the existing models use a medical image or a signal for detecting PD. But in this work, different multi-modality images and signals are used as input to the proposed deep learning model to identify Parkinson's disease better accurately.

3. PROPOSED METHODOLOGY

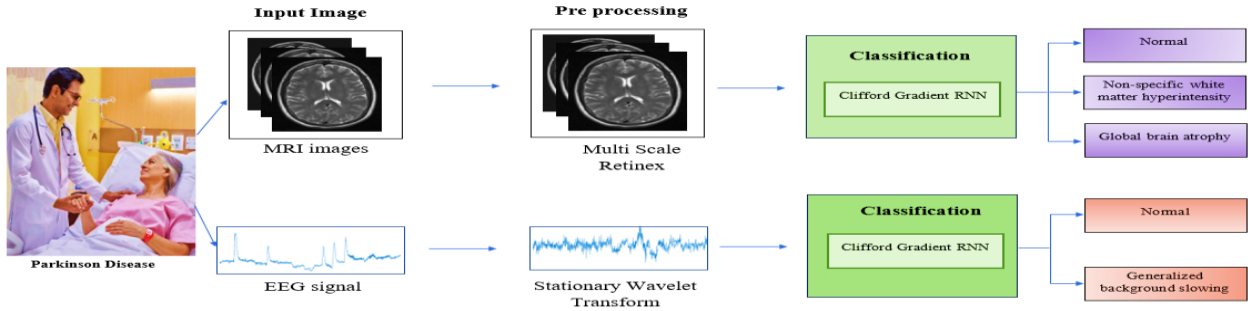This research proposes a novel Cliff-PD to detect Parkinson's disease using a Clifford gradient RNN classifier with model images like MRI and EEG signals. The MRI images are initially denoised using MSR, and EEG signals are pre-processed using Stationary Wavelet Transform filters to reduce noise artifacts. Then, the Clifford gradient RNN is employed to classify normal, non-specific white matter hyperintensity and global brain atrophy using MRI images. Furthermore, the Clifford gradient RNN is employed to classify the normal, generalized background slowing using an EEG signal – the overall performance of the proposed Cliff-PD methodology displayed in Fig. 1.

Fig. 1 – The overall performance of the proposed methodology.

3.1. DATASET DESCRIPTION

This study tests the recommended strategies utilizing two open-source EEG datasets. The first dataset was given by the University of San Diego in California (37,38). We will refer to this dataset as the San Diego dataset for convenience. While the data were being obtained, the individuals of this dataset were instructed to unwind by staring at a cross on a screen. The dataset contains two groups. EEGs from 16 healthy individuals comprise the first group, whereas those from 15 PD patients comprise the second. When the mini-mental state examination (MMSE) and the North American adult reading Test (NAART) were used to assess the right-handedness, gender, age, and cognitive abilities of the PD patients, the results were very similar to those of the HC. The average length of each patient's disease was 4.5–3.5 years, with Hoehn and Yahr ratings II and III ranging from moderate to severe. EEG data from PD patients were collected on two days, both with and without treatment—the healthy subjects produced just one volunteer. EEG data was recorded at 512 Hz for at least three minutes using a 32-channel Biosemi active EEG device. All the data were re-referenced to the common average once the means for each channel were extracted using EEGLAB. A 0.5 Hz high-pass filter was used to minimize low-frequency drift.

Due to restrictions on the use of patient data, the analyzed fMRI datasets are not accessible to the general public. Using private online cloud storage, the corresponding author will make the study protocol and each participant's de-identified raw fMRI data available to researchers upon reasonable request for repeatability assessments.

3.2. DENOISING

In the denoising stage, the MRI images are pre-processed utilizing MSR, and the EEG signal is pre-processed using stationary wavelet transform filters to reduce the noise artifacts.

3.2.1. Image denoising

Pre-processing has an important part in improving the numerous changes in MRI images and decreasing noise. Multi-scale Retinex is effective in reducing noise while preserving important image details. By operating at multiple scales, it can handle both small and large details present in the image. some other denoising methods, Multi-scale Retinex is capable of reducing noise without significantly blurring the image. It maintains edge sharpness and overall image clarity. The MSR image processing algorithm expands SSR and is motivated by human vision. The single-scale Retinex technique, which is a linear weighted of the MSR algorithm, is precisely represented by the following formula.

$$N_i(y,z) = \sum_{k=1}^{M} W_K \left\{ \log J_j(y,z) - \log \left[F_k(y,z)^* J_j(y,z) \right] \right\}, \quad (1)$$

where W_K is the weight associated with the kth scale and the general value is 3, m is the number of scales, which represents the wraparound function at scale F_K. where $N_j(y, z)$ is the intensity value of the y and z coordinates for the jth color channel of the RGB model. The value of K is usually 3, and $W_1 = W_2 = W_3 = 1/3$. In addition, the result shows taking 15,80,120 respectively. image improvement for the original color image after coping with minimal light. The following provides the surround function:

$$F_m(y, z) = K_m e^{-(y^2 + z^2)/c_n^2}, \quad (2)$$

where the normalization factor $K_m = 1 / (\sum_y \sum_z F(y, z))$ and c_n are the scales that control the extent of the surround. Most weights can be fitted into three scales, and images can have equal weights. This is more of an experimental than a theoretical exercise because it is not known how an image will scale up in real-world scenes. It is possible to change the weights so that either color rendition or dynamic range compression is given more weight.

3.2.2. Signal denoising

The stationary wavelet transform (SWT) solves the translation invariance problem of the discrete wavelet transformations (DWT). The length of the sequences produced by the high and low pass filters is the same at every level. Because SWT is time-invariant, it preserves the exact temporal properties of the original signal at every stage of decomposition. To minimise repetition and increase robustness, the filter taps in SWT are separated by zeros as opposed to decimal points. The input EEG signal (I) index set is considered as $2D[x, y], I[x, y]$ describes the xth column and y^{th} row pixel.

To determine the approximation coefficients (LL), vertical coefficients (LH), horizontal coefficients (HL), and diagonal coefficients (HH), in that sequence, SWT performs first level 2D-SWT based on the EEG signal. Every sub band coefficient of the wavelet transform was recovered as two wavelet sub bands from the EEG signal using 2DSWT. The following is a representation of the 2DSWT's approximate and detailed coefficients:

$$\tilde{C}_{i+1,j,n} = \sum_{U=-\infty}^{\infty} h(u)h(u)\tilde{C}_{i,j+2^i,n+2^i V}, \tag{3}$$

$$\tilde{d}_{1,i+1,j,n} = \sum_{U=-\infty}^{\infty} h(u)h(v)\tilde{d}_{1,i,j+2^i,n+2^i V}, \tag{4}$$

$$\tilde{d}_{2,i+1,j,n} = \sum_{U=-\infty}^{\infty} h(u)h(v)\tilde{d}_{2,i,j+2^i,n+2^i V}, \tag{5}$$

$$\tilde{d}_{3,i+1,j,n} = \sum_{U=-\infty}^{\infty} h(u)h(v)\tilde{d}_{3,i,j+2^i,n+2^i V}, \tag{6}$$

where the approximation and detailed coefficients are denoted by $C_{i,j}$ and $d_{i,j}$, respectively. The concatenation of the four subbands following the 2DSWT decomposition is consistently exactly the same size as the original EEG signal.

3.3. CLASSIFICATION

Clifford gradient RNN provides a classification of Parkinson disease such as normal, non-specific white matter hyperintensity and global brain atrophy. Clifford gradient RNNs may be able to detect Parkinson's disease symptoms early and predict its progression, allowing early intervention and treatment. Parkinson's disease is characterized by progressive motor symptoms that change over time. Clifford gradient RNNs can capture the temporal dynamics of these symptoms, allowing for a better understanding and classification of the disease stages. In addition, it has been used to solve several technical and scientific challenges in fields including neural processing, robot and computer vision, and control issues. Recently, researchers have begun to pay more attention to Clifford-valued NN (CVNN) models as a potential new research area for both theoretical and applied studies. However, CVNN models frequently exhibit more intricate dynamic properties than complex-valued, CVNN models, and real-valued. There are still few studies on CVNN dynamics because of the issue with multiplication's commutativity with respect to Clifford numbers.

$$\partial_x f(x) = E^i \partial_{x^i} f(x) = E^i f_i(x), \tag{7}$$

where $f_i(x) := \partial_{x^i} f(x)$ is the partial derivative of f with respect to x^i, evaluated at x. Specifically, if f: $G_n^1 \to R$ is a scalar-valued function of a 1-D vector, then its can be given by $\partial_x f(x) = e^i \partial_{x^i} f(x) = e^i f_i(x)$.

Consider the trivial function f: $X \to X$, $X \epsilon G_n$, then $\partial_X f(X) = e^i \partial_{x^i} x^j E_j = 2^n$, where n is the dimension of algebra. From the associativity of the geometric product, the following assumptions are derived:

1) $\partial_X XA = 2^n A$, where $A \in G_n$.
2) $\partial_X AX = E^i AE_i \neq 2^n A$.

$$\partial_X AX = E^i \partial_{x^i} Ax^j E_j = E^i AE_j = \frac{E_i AE_i}{E_i E_i} \neq 2^n A, \tag{8}$$

The physical foundation for a multispectral image pixel's spectral mClifford (X), is the multi-vector function of the spectrum intensity. Additionally, it may convey any spectral strength as well as the relationships between several spectra. The norm of the spectral gradient mClifford(X) can be defined as,

$$\| mClifford \| = \sqrt{\partial_X f(X) \overline{\partial_X f(X)}} =$$
$$= \sqrt{\sum_r |\langle \partial_X f(X) \rangle r|^2}. \tag{9}$$

The spectral gradient mClifford(X) is a Clifford algebra.

4. RESULT AND DISCUSSION

The innovative setup of this study was implemented by MATLAB, a deep learning toolbox. In this result analysis, the input MRI images are classified into three types: normal, Non-specific white matter hyperintensity, and global brain atrophy, and the EEG signal is classified into two types: normal and generalized background slowing. The following deep toolbox operation was performed in MATLAB.

1. Image input layer with the input size property set to 28,28,1;
2. convolution 2d layer;
3. batch Normalization layer;
4. relu Layer;
5. fully Connected Layer with the output size property set to 10;
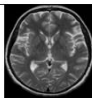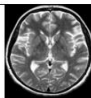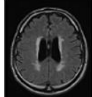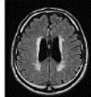6. SoftMax layer;
7. classification layer.
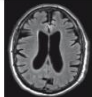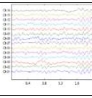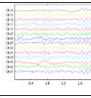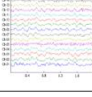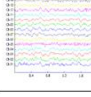
Fig. 2 – The outcomes of the suggested Cliff-PD models.

The following deep toolbox operation was performed in MATLAB. The term "Cliford Gradient RNN" might refer to a specific type of recurrent neural network (RNN) architecture that incorporates Clifford algebra or utilizes gradient-based RNN techniques. If this research based RNN architecture, need to implement it yourself using MATLAB's Deep Learning toolbox by creating a neural network layer or model.

In Fig 2 simulation results of the proposed Cliff-PD model with MRI and EEG signal. The MRI images are denoised using MSR and EEG signal are pre-processed using Stationary Wavelet Transform filters are reducing the noise artifacts. The Clifford gradient RNN is employed to classifying the normal, Non-specific white matter hyperintensity, and global brain atrophy using MRI images. Furthermore, the Clifford Gradient RNN is employed to classifying the normal, generalised background slowing using EEG signal.

4.1. PERFORMANCE ANALYSIS

Performance analysis for this study was performed using specificity, accuracy, recall, precision, and F1 score.

$$\text{accuracy} = \frac{TP+TN}{TP+TN+FP+FN} \tag{10}$$

$$\text{Specificity} = \frac{TN}{TN+FP}, \tag{11}$$

$$\text{Precision} = \frac{TP}{TP+FP}, \tag{12}$$

$$recall = \frac{TP}{TP+FN}, \qquad (13)$$

$$f_1 = 2\frac{precision*recall}{precision+recall}, \qquad (14)$$

where FP indicates false-positives, FN indicated false-negatives, TP indicates true-positives and TF indicate true-negatives respectively.

Table 1

The performance metrices for MRI and EEG signal of proposed methodology

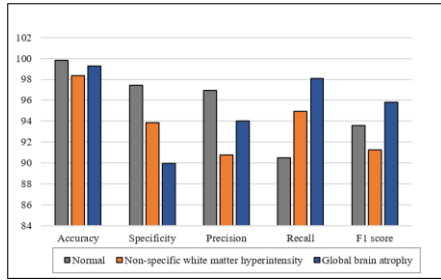| Input	Classes	Accuracy	Specificity	Precision	Recall	F1 score
MRI images	Normal	99.84	97.46	96.95	90.48	93.57
	Non-specific white matter hyperintensity	98.37	93.85	90.76	94.95	91.28
	Global brain atrophy	99.28	89.94	94.02	98.09	95.82
EEG signal	Normal	98.83	95.06	96.09	88.26	90.37
	Generalised background slowing	99.59	97.49	89.83	87.40	95.68

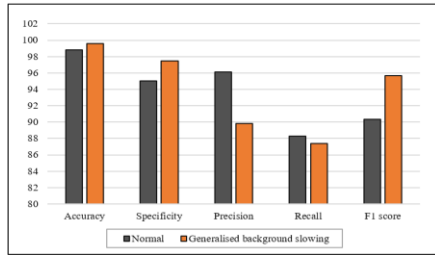Fig. 3 – Performance metrics for MRI images of three classes.

Fig. 4 – Performance metrics for EEG signal of two classes.

Figure 3 represents the performance analysis of Cliff-PD method, it includes three classes such as normal, Non-specific white matter hyperintensity, and global brain atrophy. Figure 4 represents the performance analysis of Cliff-PD method, it includes two classes such as normal, generalised background slowing.
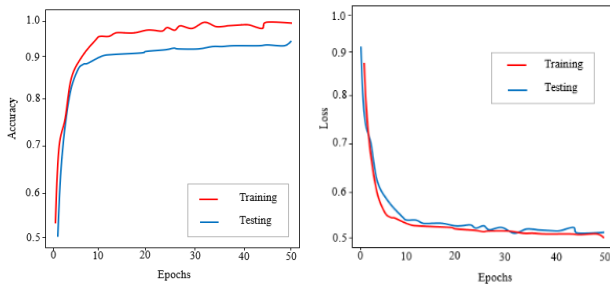
(a) Accuracy.   (b) Loss.

Fig. 5 – Training and testing are proposed in Cliff-PD.

Table 1 shows the results in terms of overall accuracy. The proposed Cliff-PD method yields an accuracy of 99.84 %, 98.37 %, and 99.28 % for normal, Non-specific white matter hyperintensity and global brain atrophy from the MRI images. The proposed Cliff-PD method achieved the accuracy of 98.83 % and 99.59 % for normal, generalised background slowing from the EEG signal.

Figure 5a shows the Cliff-PD method has better accuracy in training and testing, Figure 5b displays the loss. Performance is evaluated by specificity, recall, precision,

and F1 score, and the Cliff-PD method an achieves 99.18 % accuracy.

4.2. COMPARATIVE ANALYSIS

The traditional neural networks and the Clifford gradient RNN are also compared in this division. Comparing the performance of Clifford Gradient RNN with existing methods shows more than existing methods. This comparative analysis compares three existing DL algorithms with the Clifford gradient RNN.

Table 2 demonstrates that the findings in terms of total accuracy rate were attained. Traditional networks like DenseNet, AlexNet, and RNNs perform less accurately than Clifford Gradient RNNs. The accuracy obtained by CNN, Dense Net, GoogleNet, and Mobile Net is 94.28%, 89.27%, 91.59%, and 98.38%, respectively, according to Fig. 6.

Table 2

The comparison between traditional DL networks

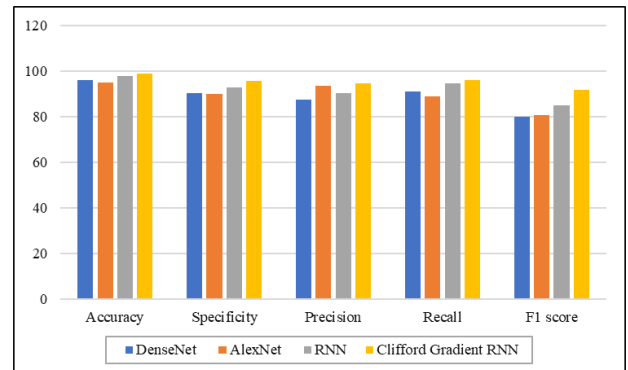| Techniques	Accuracy	Specificity	Precision	Recall	F1 score
DenseNet	96.26	90.47	87.62	91.06	79.94
AlexNet	95.19	89.92	93.73	88.94	80.73
RNN	97.84	93.04	90.27	94.81	85.06
Clifford Gradient RNN	99.18	95.72	94.83	96.27	91.95

Fig. 6 – Comparison of traditional deep learning models.

Dense net, AlexNet, RNN, and Clifford Gradient RNN all achieved specificities of 96.26 %, 95.19 %, 97.84 %, and 99.18 %, respectively. The Clifford gradient RNN outperforms the previous models in terms of accuracy.

To compare the effectiveness of various techniques, based on the efficacy of classification, previous models were compared using a performance criterion. Comparing the Cliff-PD to SVMs, AlexNet's and CROWD autoencoder the accuracy range is improved overall by 5.38 %, 10.36 % and 3.2 % respectively. Our Cliff-PD is better than other approaches, as shown in Table 3.

Table 3
The comparison of proposed Cliff-PD and the existing models

Authors	Techniques	Accuracy
Z.K. Senturk, [11]	SVMs	93.84 %
S. Sivaranjini, C.M. Sujatha [13]	AlexNet's	88.9 %
M. Masud et al. [14]	CROWD autoencoder	96 %
Proposed	Cliff-PD	99.18 %

5. CONCLUSION

This research proposes a novel Cliff-PD to detect Parkinson's disease using a Clifford gradient RNN classifier with model images like MRI and EEG signals. The MRI images are initially denoised using MSR, and EEG signals are pre-processed using Stationary Wavelet Transform filters to reduce noise artifacts. Then, the Clifford gradient RNN is employed to classify the normal, non-specific white matter hyperintensity and global brain atrophy using MRI images. Furthermore, the Clifford gradient RNN is employed to classify the normal, generalized background slowing using an EEG signal. The performance of the proposed Cliff-PD method achieved an accuracy of 99.18 %. Comparing the Cliff-PD to SVMs, AlexNet's and CROWD autoencoders' accuracy ranges are improved overall by 5.38 %, 10.36 %, and 3.2 %, respectively. Deep fine-tuning of the advanced CNN model can be done using the proposed methodology to improve performance. Due to the rapid development of deep learning architectures, the physician won't have to expend as much time and effort in the future on making an objective diagnosis of Parkinson's disease.

ACKNOWLEDGEMENTS

REFERENCES

1. R. Sharma, A. Kumar, R. Ray, *Latest progresses and methods used to treat Parkinson's disease*, International Journal of Innovative Science and Research Technology, **7**, *9*, pp. 574–582 (2022).
2. A. Becerra-Calixto, A. Mukherjee, S. Ramirez, S. Sepulveda, T. Sinha, R. Al-Lahham, N. De Gregorio, C. Gherardelli, C. Soto, *Lewy body-like pathology and loss of dopaminergic neurons in midbrain organoids derived from familial Parkinson's disease patients*, Cells, **12**,*4*, p. 625 (2023).
3. E. Tolosa, A. Garrido, S.W. Scholz, W. Poewe, *Challenges in the diagnosis of Parkinson's disease*, The Lancet Neurology, **20**, *5*, pp. 385–397 (2021).
4. A. Lakshmi, *A disease prediction model using spotted hyena search optimization and Bi-LSTM*, Rev. Roum. Sci. Techn. – Électrotechn. et Énerg., **68**, *1*, 113–118 (2023).
5. T. Foltynie, S. Gandhi, C. Gonzalez-Robles, M.L. Zeissler, G. Mills, R. Barker, J. Carpenter, A. Schrag, A. Schapira, O. Bandmann, S. Mullin, *Towards a multi-arm multi-stage platform trial of disease modifying approaches in Parkinson's disease*, Brain, **146**, *7*, 2717–2722 (2023).
6. P. Mahlknecht, K. Marini, M. Werkmann, W. Poewe, K. Seppi, *prodromal Parkinson's disease: hype or hope for disease-modification trials?*, Translational Neurodegeneration, **11**, *1*, pp. 1–13 (2022).
7. A. Topor, D. Ulieru, C. Ravariu, F. Babarada, *Development of a New One-Eye Implant By 3d Bioprinting Technique*, Rev. Roum. Sci. Techn. – Électrotechn. et Énerg., **68**, *2*, pp. 247–250 (2023).
8. G.G. Tolun, Y.A. Kaplan, *Development of Backpropagation Algorithm for Estimating Solar Radiation: A Case Study in Turkey*, Rev. Roum. Sci. Techn. – Électrotechn. et Énerg., **68**, *3*, pp. 313–316 (2023).
9. Y. Li, Z. Zhu, J. Chen, M. Zhang, Y. Yang, P Huang, *Dilated perivascular space in the midbrain may reflect dopamine neuronal degeneration in Parkinson's disease*, Frontiers in Aging Neuroscience, **12**, 161 (2020).
10. K.L. Chou, P. Dayalu, R.A. Koeppe, S. Gilman, C.C. Spears, R.L. Albin, V. Kotagal, *Serotonin transporter imaging in multiple system atrophy and Parkinson's disease*, Movement Disorders, **37**,*11*, pp. 2301–2307 (2022).
11. A.K. Schalkamp, K.J. Peall, N.A. Harrison, C. Sandor, *Wearable movement-tracking data identify Parkinson's disease years before clinical diagnosis*, Nature Medicine, **29** pp. 2048–2056 (2023).
12. Z.K. Senturk, *Early diagnosis of Parkinson's disease using machine learning algorithms*. Medical hypotheses, **138**, 109603 (2020).
13. H. Gunduz, *Deep learning-based Parkinson's disease classification using vocal feature sets*, IEEE Access, **7**, pp. 115540–115551 (2019).
14. S. Sivaranjini, C.M. Sujatha, *Deep learning-based diagnosis of Parkinson's disease using convolutional neural network*. Multimedia Tools and Applications, **79,** pp. 15467–15479 (2020).
15. M. Masud, P. Singh, G.S. Gaba, A. Kaur, R. Alroobaea, M. Alrashoud, S.A. Alqahtani, *CROWD: crow search and deep learning-based feature extractor for classification of Parkinson's disease*, ACM Transactions on Internet Technology (TOIT), **21**,*3*, pp. 1–18 (2021).
16. M. Wodzinski, A. Skalski, D. Hemmerling, J.R. Orozco-Arroyave, E. Nöth, *Deep learning approach to Parkinson's disease detection using voice recordings and convolutional neural network dedicated to image classification*, 41st Annual International Conference of the IEEE Engineering in Medicine and Biology Society (EMBC), pp. 717–720 (2019).
17. A.M. Elshewey, M.Y. Shams, N. El-Rashidy, A.M. Elhady, S.M. Shohieb, Z. Tarek, *Bayesian optimization with support vector machine model for Parkinson disease classification*, Sensors, **23**, *4*, 2085 (2023).
18. X. Yang, Q. Ye, G. Cai, Y. Wang, G. Cai, *PD-ResNet for classification of Parkinson's disease from gait*, IEEE Journal of Translational Engineering in Health and Medicine, **10**, pp. 1–11 (2022).
19. I. Gupta, V. Sharma, S. Kaur, A.K. Singh, *PCA-RF: an efficient Parkinson's disease prediction model based on random forest classification*, arXiv preprint arXiv:2203.11287 (2022).
20. H.A. Carvajal-Castaño, P.A. Pérez-Toro, J.R. Orozco-Arroyave, *Classification of Parkinson's disease patients – a deep learning strategy*, Electronics, **11**, *17*, p. 2684 (2022).
21. A. Govindu, S. Palwe, *Early detection of Parkinson's disease using machine learning*, Procedia Computer Science, **218**, pp. 249–261 (2023).
22. K.B. Shah, S. Visalakshi, R. Panigrahi, *Seven class solid waste management-hybrid features based deep neural network*, International Journal of System Design and Computing, **01**, *01*, pp. 1–10 (2023).
23. B. Saravanan, M. Duraipandian, V. Pandiaraj, *An effective possibilistic fuzzy clustering method for tumor segmentation in MRI brain image*, Sixth International Conference on I-SMAC (IoT in Social, Mobile, Analytics, and Cloud) (I-SMAC, IEEE), pp. 823–827 (November 2022).
24. R.R. Sathiya, S. Rajakumar, J. Sathiamoorthy, *Secure blockchain-based deep learning approach for data transmission in IOT-enabled healthcare system*, International Journal of Computer and Engineering Optimization, **01**, *01*, pp. 15–23 (2023).
25. P. Naveen, P. Sivakumar, *A deep convolution neural network for facial expression recognition*, Journal of Current Science and Technology, **11**, *3*, pp. 402–410 (2021).
26. S. Zafar, N. Iftekhar, A. Yadav, A. Ahilan, S. N. Kumar, A. Jeyam, *An IoT method for telemedicine: lossless medical image compression using local adaptive blocks*, IEEE Sensors Journal, **22**, *15*, pp. 15345–15352 (2022).
27. J. Angel Sajani, A. Ahilan, *Classification of brain disease using deep learning with multi-modality images*. Journal of Intelligent & Fuzzy Systems, (Preprint), **45**, *2*, pp. 3201–3211 (2023).